Applied Catalysis B: Environmental 195 (2016) 121–131

Contents lists available at ScienceDirect

Applied Catalysis B: Environmental

journal homepage: www.elsevier.com/locate/apcatb

On the enhancing effect of Ce in Pd-MOR catalysts for NO_x CH_4-SCR: A structure-reactivity study

Acácio Nobre Mendes[a,b], Vladimir L. Zholobenko[c,d], Frédéric Thibault-Starzyk[c], Patrick Da Costa[b,e], Carlos Henriques[a,*]

[a] Centro de Química Estrutural, Instituto Superior Técnico, Universidade de Lisboa. Av. Rovisco Pais, 1049-001 Lisboa, Portugal
[b] Sorbonne Universités, UPMC Univ. Paris 06, UMR 7190, Institut Jean le Rond d'Alembert, F-75005, Paris, France
[c] Laboratoire Catalyse et Spectrochimie, UMR 6506, CNRS-ENSICAEN, Université de Caen, 6, boulevard du Maréchal-Juin, 14050 Caen, France
[d] Keele University, Keele, Staffordshire, ST5 5BG, UK
[e] CNRS, UMR 7190, Institut Jean le Rond d'Alembert, F-78210, Saint-Cyr l'Ecole, France

ARTICLE INFO

Article history:
Received 7 March 2016
Received in revised form 2 May 2016
Accepted 4 May 2016
Available online 6 May 2016

Keywords:
NO_x HC-SCR
Methane
MOR
Palladium
Cerium

ABSTRACT

The effect of palladium and cerium species on the selective catalytic reduction (SCR) of NO_x using methane as reductant (NO_x CH_4-SCR) has been investigated using Pd-HMOR and PdCe-HMOR system. The catalysts have been characterised by H_2-TPR, DRS UV–Vis, TEM/EDS and FTIR using CO and pyridine as probe molecules. The oxidation of NO and CH_4-SCR catalytic tests have been conducted using monometallic and bimetallic formulations.

Above 0.3 wt.% Pd, the increase in Pd loading leads to a decrease in NO_x selectivity towards N_2, with the formation of N_2O, and a decrease in the CH_4 selectivity towards SCR, due to CH_4 direct combustion. H_2-TPR and FTIR-CO studies indicate that palladium is stabilised as Pd^{2+} in ion-exchange position, probably in two different sites within the MOR framework.

The addition of cerium to Pd-HMOR enhances its catalytic performance for NO_x CH_4-SCR. With 1 wt.% Ce, both NO_x conversion into N_2 and CH_4 selectivity towards SCR have increased. Small CeO_2 clusters interacting with palladium are likely to play a major role in this catalytic reaction. The number of such species increases up to Ce loading of *ca.* 2 wt.%. However, above 3 wt%, NO_x conversion values decrease with Ce loading, which is attributed to the formation of bulk CeO_2 species not interacting with palladium.

1. Introduction

Over the recent decades, many countries devoted considerable resources to mitigating the impact of air pollution. Nitrogen oxides (NO_x) are one of the pollutants associated with air pollution and road transportation sector is known to be one of the major contributors to the NO_x emissions. In 2012 this sector was responsible for about 31% of the total emissions of NO_x in the European Union (EU), more than 10.7 Mton [1]. Several directives have been published over the years by the EU imposing increasingly tough restrictions on NO_x emissions. The most recent directive, known as EURO 6 standard, came into force on 1st September 2014 for the approval of vehicles, and from 1st January 2015 for the registration and sale of new types of cars, imposing a drastic reduction on NO_x emissions for heady-duty and light passenger compression ignition engines (see Table 1).

Highly effective systems based on the so-called "3-way" catalysts have been successfully used by the automotive industry in order to simultaneously eliminate the harmful emissions (NO_x, CO and unburned hydrocarbons—HC) from vehicle engines that work in stoichiometric air-to-fuel ratio (positive ignition engines, typically for gasoline vehicles) [3]. However, for lean-burn engines, which work in excess of oxygen (compression ignition engines, typically diesel vehicles), this technology is not effective for eliminating NO_x emissions.

A promising technology that has been developed to address this issue is the selective catalytic reduction of NO_x with hydrocarbons (HC-SCR) [3,4]. This technology aims to use unburned hydrocarbons contained in the exhaust gases as reductant in order to reduce NO_x to N_2, leading to the simultaneous removal of NO_x and HC, which appears to be particularly suitable for natural gas powered vehicles (NGVs). It is expected that the number of NGVs would significantly increase in the coming years. According to the NGV Global Associa-

* Corresponding author.
E-mail address: carlos.henriques@tecnico.ulisboa.pt (C. Henriques).

http://dx.doi.org/10.1016/j.apcatb.2016.05.004
0926-3373/

Table 1
HC and NO_x emissions for heavy-duty and light passengers vehicles, from Euro 1 to Euro 6 standards [2].

	Heavy-duty		Light passengers (compression ignition)		Light passengers (positive ignition)		
	HC (g/kWh)	NO_x (g/kWh)	HC + NO_x (g/km)	NO_x (g/km)	HC (g/km)	HC + NO_x (g/km)	NO_x (g/km)
Euro 1 (1992)	1.1	8	0.97	–	–	0.97	–
Euro 2 (1996)	1.1	7	0.7	–	–	0.5	–
Euro 3 (2000)	0.66	5	0.56	0.5	0.2	–	0.15
Euro 4 (2005)	0.46	3.5	0.3	0.25	0.1	–	0.08
Euro 5 (2009)	0.46	2	0.23	0.18	0.1	–	0.06
Euro 6 (2014)	0.13	0.4	0.17	0.08	0.1	–	0.06

tion, the number of NGVs worldwide has increased from about 7.4 million (2007) to 16.7 million (2012) [5]. For these reasons, the continuous study of after-treatment systems capable of mitigating the pollution from these vehicles, namely NO_x emissions, is pertinent and necessary.

For NGVs, the most abundant hydrocarbon in the exhaust gases is CH_4. Zeolite-based catalysts containing different metals have been reported as active materials for the selective catalytic reduction of NO_x with methane (CH_4-SCR). Cobalt-containing zeolites, introduced by Li and Armor as active catalysts for CH_4-SCR [6], have been widely studied by the scientific community [7–11]. This research has significantly contributed to the understanding of the nature of active species involved in this reaction, as well as the important parameters that influence NO_x CH_4-SCR reaction, such as, temperature, $[CH_4]/[NO]$ feed ratio, water feed content, *etc*. It is known that the use of bimetallic formulations leads to a better catalytic performance. Many studies on bimetallic zeolite-based catalysts have been conducted, including Pd/Co [12–18], Pt/Co [19,20], In/Co [21–23], La/Co [24], Zn/Co [25], Ag/Co [26] and Mn/Co [27]. However, the use of Co in final products such as catalytic converters may be restricted for legal reasons. Many compounds, including cobalt (II) chloride, carbonate, acetate, nitrate and sulphate are chemical products which are included in the candidate list of substances of very high concern for authorisation (REACH regulation) [28]. Some of these, namely cobalt (II) diacetate and cobalt (II) dinitrate, are commonly used in the preparation of Co-zeolite catalysts. Though their use is not forbidden, the EU suppliers of products that contain these substances in a concentration above 0.1 wt.% need to declare it to the appropriate authorities, which may discourage companies to invest in the development of this type of technology.

Zeolites-based catalysts containing metals other than Co are also claimed to be active in CH_4-SCR. Nishizaka and Mizono [29] published the first report describing Pd-zeolites as active catalysts in this reaction. Since then, several studies have been conducted in order to move forward to a better understanding of this system. As in the case of the Co-based systems, the use of a second metal in the Pd-based catalyst to enhance its performance has been widely reported, *e.g.* Pd/Pt [30], Pd/In [31,32], and Pd/Ce [33–35] systems.

Compared to platinum and indium, the use of cerium may represent an advantage from the economical point of view. Promising results for Pd/Ce system have been presented already [34,35]; however, the role of various Pd and Ce species in the NO_x CH_4-SCR requires further investigation. The aim of this work is to further understand the structure-reactivity relationship in the Pd/Ce zeolites, in particular the role of different metal species in the enhancement of their catalytic performance.

2. Experimental part

2.1. Catalysts preparation

Catalysts were prepared from CBV21A zeolite (NH_4MOR), with Si/Al = 10 supplied by Zeolyst International. Monometallic Pd-zeolites were obtained from by NH_4MOR by ion-exchanging the zeolite with $[Pd(NH_3)_4](NO_3)_2$ aqueous solutions of adequate concentration, at room temperature, for 24 h. In a typical preparation, 6 g of the parent zeolite was mixed under stirring with 300 mL of a Pd complex solution (*e.g.* 0.15 wt.% prepared by dilution of the original 10 wt.% aqueous solution of $[Pd(NH_3)_4](NO_3)_2$, Sigma-Aldrich, 99.99%). The ion-exchanged samples were recovered by centrifugation and dried overnight at 90 °C. Next, Pd-zeolites were calcined under air flow at 500 °C for 1 h (1 °C/min temperature ramp). Bimetallic PdCe-zeolites were obtained from Pd(0.3)-HMOR, by incipient wetness impregnation, using solutions of adequate concentration prepared from $Ce(NO_3)_3{\cdot}6H_2O$ (Fluka, 99% purity). Samples were dried overnight at 90 °C and finally calcined at 500 °C for 8 h (5 °C/min temperature ramp). Monometallic Ce(2)-HMOR was obtained from NH_4MOR, following the same procedure as previously described. HMOR form was prepared from NH_4MOR via calcination at 500 °C, for 8 h (5 °C/min temperature ramp). The chemical composition data for the catalysts investigated in this work are presented in Table 2.

Table 2
Chemical composition of the catalysts obtained by ICP-OES analysis.

Catalyst**	Al (wt.%)	Pd (wt.%)	Ce (wt.%)	ER_{Pd}* (%)	ER_{Ce}* (%)
Pd(0.15)-HMOR	3.3	0.16	–	2.4	–
Pd(0.3)-HMOR	3.3	0.36	–	5.5	–
Pd(0.5)-HMOR	3.3	0.55	–	8.4	–
Pd(0.7)-HMOR	3.3	0.75	–	11.7	–
Pd(0.3)Ce(1)-HMOR	3.3	0.35	0.8	5.4	13.7
Pd(0.3)Ce(2)-HMOR	3.4	0.29	1.9	4.3	32.2
Pd(0.3)Ce(3)-HMOR	3.5	0.39	2.8	5.6	46.0
Pd(0.3)Ce(5)-HMOR	2.9	0.27	4.8	4.8	97.1
Pd(0.3)Ce(10)-HMOR	2.8	0.27	9.1	4.8	185.3
Ce(2)-HMOR	3.3	–	2.1	–	36.6

* ER – Exchange rate (assuming 2+ and 3+ charges for Pd and Ce, respectively).
** Numbers in parentheses indicate theoretical wt.% of Pd and Ce.

2.2. Catalysts characterisation

Temperature programmed reduction under hydrogen (H_2-TPR) was performed by contacting a catalyst sample (*ca.* 100 mg) with a mixture of H_2 (5 vol.%)/Ar and heating it up to 950 °C using a ramp of 7.5 °C/min. Hydrogen consumption was measured with a thermal conductivity detector. Water was removed using a dry ice cooled trap.

Diffuse reflectance UV–Vis spectroscopy (DRS UV–Vis) was performed using a *Varian Cary 5000 UV*– spectrophotometer equipped with a Praying Mantis accessory. Spectra were collected at room temperature, using calcined samples (range 200–800 nm, scan rate of 600 nm/min, 1 nm data interval, SBW = 4 nm) and presented using the Schuster-Kubelka-Munk (SKM) function, F(R)—see Eq. (1).

$$F(R) = \frac{(1-R)^2}{2R} \quad (1)$$

R is the ratio of the intensity of the light reflected by the sample to the one reflected by a standard. In order to minimise the

effect of zeolite framework absorption, a HMOR sample was used as standard.

Transmission electron microscopy (TEM) was performed on a *JEOL JEM 2010* microscope (LaB6 cannon) operating at 200 kV. Prior to TEM measurements, samples were crushed and then dispersed in ethanol and deposited onto a carbon-coated copper TEM grid. Energy-dispersive X-ray spectroscopy (EDS) was also performed (probe PGT-Bruker).

CO adsorption monitored by FTIR spectroscopy was performed in order to evaluate the state of Pd and Ce species. The spectra were collected using a Nicolet 6700 FTIR spectrometer equipped with a DTGS detector (400–4000 cm^{-1}, 128 scans, 4 cm^{-1} resolution). Self-supported wafers of the calcined catalysts (*ca.* 10 mg/cm^2) were pre-treated by heating to 400 °C at 3 °C/min, then holding for 30 min under vacuum ($P < 10^{-5}$ torr, cell with CaF_2 windows). Next, samples were reduced at 400 °C, for 1 h, under 100 torr of H_2. After reduction, the cell was evacuated during 10 min to $P < 10^{-5}$ torr. The wafers were then cooled down to room temperature and a spectrum was collected prior to CO adsorption. 5 torr of CO was introduced into the cell and the spectra of the sample and of the CO gas phase were collected. All spectra presented were obtained by subtracting the contributions from the CO gas phase and from the reduced sample, followed by normalisation to the same weight/surface area ratio of the wafer.

Pyridine adsorption and consecutive thermodesorption studies were monitored by *in situ* FTIR in order to quantify the acidity of the samples, utilising the same experimental apparatus and pre-treatment as that previously described for the CO adsorption experiments. After pre-treatment, the wafers were cooled down to room temperature and a spectrum was collected prior to pyridine adsorption. 1 torr of pyridine was introduced into the cell and spectra of the sample and the pyridine gas phase were collected. Then, the temperature was raised to 150 °C, kept for 30 min, and another spectrum was collected. Next, the wafer was cooled down until room temperature and the cell was evacuated for 10 min ($P < 10^{-5}$ torr). A spectrum was collected. Afterwards, the temperature was raised to 50 °C, kept for 10 min, and a spectrum was collected. The same procedure was repeated every 50 °C until 400 °C. The quantification of total number of Brønsted acid sites (BAS) and Lewis acid sites (LAS) was performed through the integration of IR bands around 1545 and 1455 cm^{-1}, respectively, using molar extinction coefficients reported elsewhere [36]. Although the data from reference [36] are frequently quoted in the literature, according to our AGIR studies [37], their use may lead to a significant overestimate of the concentration of acid sites since the sample mass was not monitored during the pyridine adsorption in reference [36].

2.3. Catalytic tests

Catalytic tests were performed in a tubular *pyrex* reactor using 190 mg of the catalyst (dry basis), supported by a sintered plate (frit). Prior to reaction studies, catalysts were heated under argon flow (15 L/h) to 500 °C (5 °C/min temperature ramp) and kept at this temperature for 1 h. Then, the reactor was cooled to 300 °C whilst the reaction mixture was stabilised in the reactor by-pass. Once stable, the reaction mixture was fed to the reactor. When steady-state conditions were reached, the temperature was raised by 50 °C and the procedure was repeated up to the reaction temperature of 500 °C.

NO_x SCR tests were performed using a mixture of 1000 ppm NO, 1000 ppm CH_4 and 7 vol.% O_2 in flowing argon (total flow rate of 15 L/h, GHSV = 40000 h^{-1}). Oxidation of NO to NO_2 was performed under similar conditions, but using a mixture of 1000 ppm NO and 7 vol.% O_2 in flowing argon.

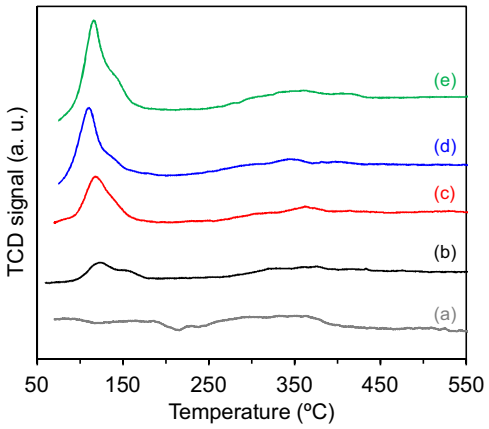

Fig. 1. H_2-TPR profile of Pd-HMOR catalysts with different Pd loadings: HMOR (a), Pd(0.15)-HMOR (b), Pd(0.3)-HMOR (c), Pd(0.5)-HMOR (d) and Pd(0.7)-HMOR (e).

The reactor outlet flow was continuously analysed using a Thermo 42C chemiluminescence detector for measuring the concentrations of NO and NO_2, an ABB EL 3020 infrared analyser to monitor CO, CO_2 and N_2O concentrations and a Pfeiffer Vacuum GSD 301 mass spectrometer to follow the concentration of CH_4 ($m/z = 15$).

For each temperature, T, NO_x conversion into N_2 was obtained using Eq. (2), CH_4 conversion into CO_2 was obtained using Eq. (3) and selectivity of methane to SCR reaction was obtained using Eq. (4).

$$x_{NO_x into N_2,T}\,(\%) = \left(1 - \frac{n_{NO,T} + n_{NO_2,T} + 2n_{N_2O,T}}{n_{NO,0} + n_{NO_2,0}}\right) \times 100\% \quad (2)$$

$$x_{CH_4 into CO_2,T}\,(\%) = \frac{n_{CO_2,T}}{n_{CH_4,0}} \times 100\% \quad (3)$$

$$S_{CH_4 toSCR,T}\,(\%) = \frac{n_{CH_4 forSCR,T}}{n_{CH_4 converted,T}} = \frac{1}{2}\frac{n_{NO,0} + n_{NO_2,0} - \left(n_{NO,T} + n_{NO_2,T} + 2n_{N_2O,T}\right)}{n_{CH_4,0} - \left(n_{CO_2,T} + n_{CO,T}\right)} \times 100\% \quad (4)$$

0 represents the initial condition (by-pass mixture) before starting the reaction. n_i represents the molar flow of component *i*.

3. Results and discussion

3.1. Effect of Pd loading

3.1.1. Temperature programmed reduction under H_2

H_2-TPR profiles of HMOR and Pd(x)-HMOR catalysts (with x = 0.15, 0.3, 0.5 and 0.7 wt.% Pd) are presented in Fig. 1. A single peak found between 80 and 180 °C can be ascribed to Pd^{2+} ions in exchange position [38–40]. The integration of this peak for each sample yields a H_2/Pd ratio close to unity, suggesting that all Pd is stabilised as Pd^{2+}.

Further analysis of the H_2-TPR profiles in the region between 80 and 180 °C (Fig. 2) reveals two Gaussian components of the reduction peak: the first centred at temperatures below 125 °C and the second above 130 °C. One possible explanation for this phenomenon might be the stabilisation of Pd^{2+} ions in different exchange positions of the MOR structure. Dedecek and Wichterlová conducted a detailed investigation of the nature of Co^{2+} ions and their occupancy in mordenite, using DRS UV–vis-NIR spectroscopy [41]. By studying Co-MOR samples, containing different amounts of Co introduced by ion-exchange, they identified three different Co

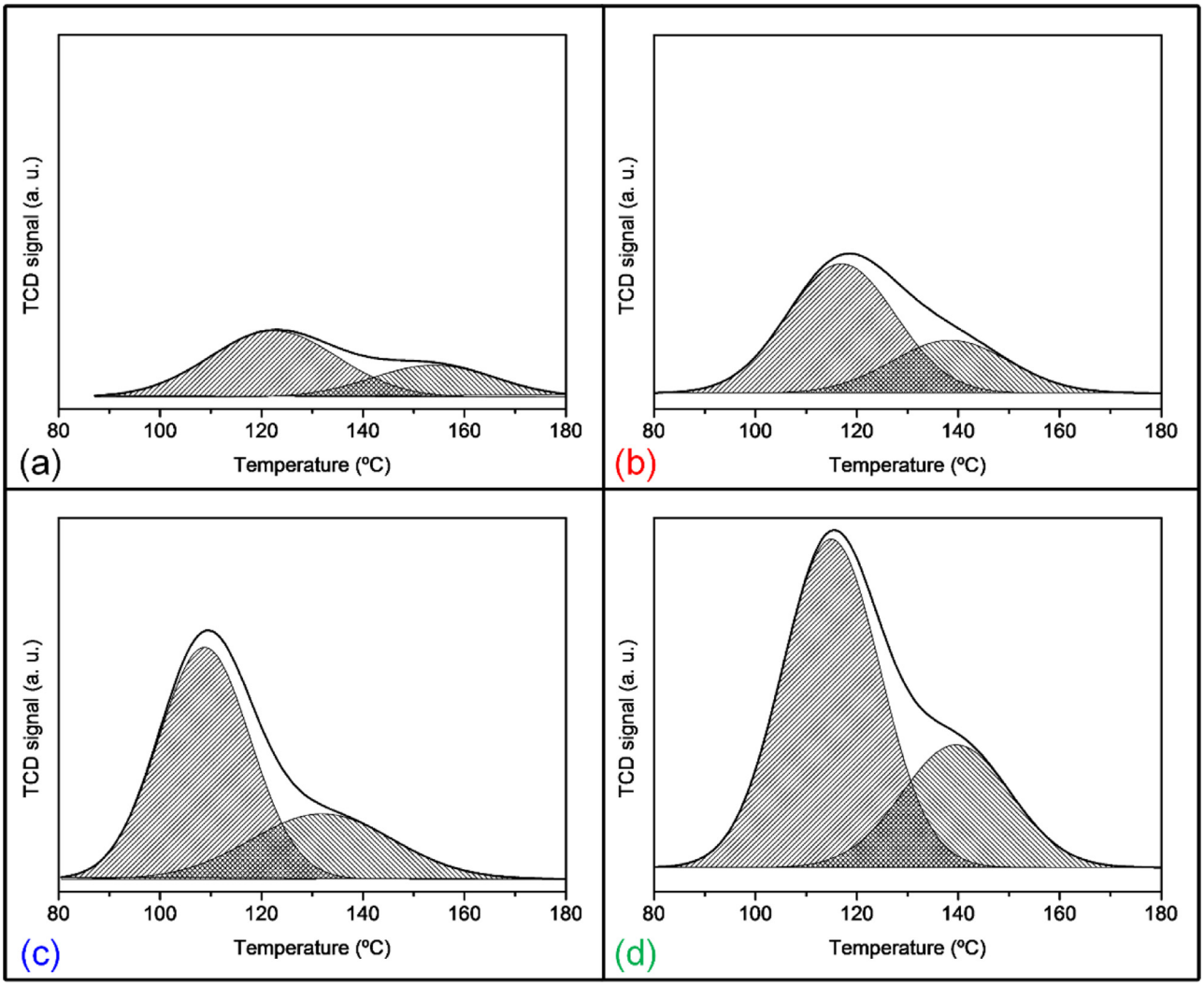

Fig. 2. Gaussian peak fitting to H_2-TPR profiles of Pd(0.15)-HMOR (a), Pd(0.3)-HMOR (**b**), Pd(0.5)-HMOR (**c**) and Pd(0.7)-HMOR (**d**).

species (α, β and γ), corresponding to different three different spectral components of DRS-UV–vis-NIR spectrum. These different Co^{2+} ions would be stabilised in specific ion-exchange sites corresponding, respectively to sites E, A and C according the nomenclature proposed by Mortier [42].

A density functional investigation conducted by Grybos et al. [43] focused on the stabilisation of Pd^{2+} ions in mordenite exchange positions corresponding to sites A, B, C, D and E proposed by Mortier [42]. The authors studied the role of Al distribution over the zeolite framework and concluded that, despite being more or less random, it has an effect on the stability of Pd^{2+} ions in each site, which is related to the number of bonds between Pd and O atoms directly connected to Al sites. Based on the calculation of the total energy associated to each configuration for Al ions distribution involved in the different sites, the authors concluded that, though Pd location in positions B, D and E do not represent a very large penalty in terms of total energy, positions A and C are the energetically most favourable locations for Pd^{2+} cations [43].

In the present work, it is not possible to describe the nature and location of different Pd^{2+} ions with the same degree of precision. Nevertheless, for each sample, the integration of the two Gaussian peaks allows to estimate the distribution of palladium as two different Pd^{2+} ions (Fig. 2, Table 3), although their exact location (for instance, 12-membered ring channels and side pockets) cannot be identified. The fraction of each of the species stabilised in the zeolite framework is almost constant (approximately 70%/30%) for all Pd loadings, resulting from a proportional increase in the concentration of both species at higher Pd loading. It should be noted that even at 0.7 wt.% of Pd, the exchange rate is relatively low (11.7%), meaning that only a small amount of exchange positions are occupied by Pd^{2+} ions.

Table 3
Quantification of the relative amount of Pd^{2+} corresponding to both reduction processes of Pd(x)-HMOR (x = 0.15, 0.3, 0.5 and 0.7) from Fig. 2.

	Gaussian peak A		Gaussian peak B	
	T (°C)	Amount of Pd^{2+}	T (°C)	Amount of Pd^{2+}
Pd(0.15)-HMOR	121	68%	153	32%
Pd(0.3)-HMOR	118	69%	141	31%
Pd(0.5)-HMOR	109	70%	132	30%
Pd(0.7)-HMOR	114	71%	136	29%

3.1.2. CO adsorption followed by FTIR spectroscopy

Fig. 3 presents the FTIR spectra of HMOR and Pd(x)-HMOR catalysts after CO adsorption. In the spectrum of HMOR sample, two bands observed at ~2220 and ~2199 cm^{-1} can be assigned to Al^{3+}-CO complexes resulting from the interaction of CO with

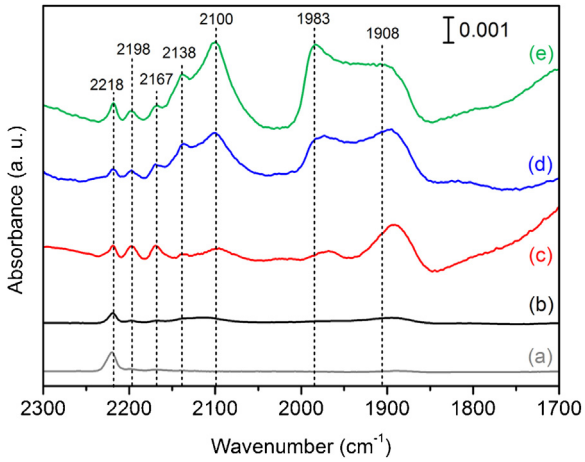

Fig. 3. FTIR spectra of reduced catalysts collected at room temperature, after exposure to 5 torr of CO: HMOR (a), Pd(0.15)-HMOR (b), Pd(0.3)-HMOR (c), Pd(0.5)-HMOR (d) and Pd(0.7)-HMCOR (e).

extra-framework Al [44–46]. These bands are also observed for all Pd(x)-HMOR catalysts.

For Pd(x)-HMOR samples, three additional groups of bands are observed between 2220 and 1890 cm^{-1}. According to Hadjiivanov and Vayssilov [44], IR bands in the 2215–2110 cm^{-1} spectral range have been attributed to linear Pd^{n+}-CO complexes. The band at ~2167 cm^{-1} can be assigned to residual Pd cations, such as Pd^{2+} [44], or to Brønsted acid sites (BAS) [31,38], whereas the band at 2140 cm^{-1} can be ascribed to Pd^{+}-CO or $Pd^{\delta+}$-CO complexes [38]. The presence of both bands suggests the existence of Pd cations or small positively charged Pd clusters, likely to be located in the vicinity of BAS, even after reduction in H_2 at 400 °C. Bands below ~2100 cm^{-1} are typical of CO interactions with metallic palladium species [44]. The bands at 2114–2100 cm^{-1} are assigned to linear Pd^0-CO complexes, which appear slightly blue-shifted for Pd(0.15)-HMOR and Pd(0.3)-HMOR. The bands between 1983 and 1892 cm-1 are attributed to bridging CO on Pd^0 clusters (two-fold and three-fold co-ordinations, the latter are found below ~1900 cm^{-1}). The low intensity of all these bands in Pd(0.15)-HMOR can be related to the low palladium content in the sample. For Pd(0.3)-HMOR, Pd(0.5)-HMOR and Pd(0.7)-HMOR catalysts, the intensity of the bands typical for Pd^0-CO complexes is significantly increased reflecting the higher contents of palladium in these samples and a higher degree of reduction to metallic palladium species. The bands attributed to bridging CO complexes on Pd^0 are blue-shifted for Pd(0.5)-HMOR and Pd(0.7)-HMOR, probably due to the larger Pd particle size (Fig. 3), which corresponds to the fact that these species are more stable in these catalysts.

3.1.3. Active species on Pd-HMOR for NO_x CH_4-SCR

The catalytic performance of Pd(x)-HMOR catalysts for NO_x CH_4-SCR was assessed at the reaction temperatures between 300 and 500 °C (Fig. 4). Pd(0.15)-HMOR presents slightly lower NO_x conversion values than the other catalysts, whereas for Pd loadings between 0.3-0.7 wt.%, all catalysts present similar values of NO_x and CH_4 conversion, with practically no formation of N_2O. However, at 500 °C, a decrease in NO_x conversion to N_2 is observed as the Pd loading increases from 0.3 to 0.7 wt.%, accompanied by an increase in both N_2O formation and CH_4 conversion. NO_x selectivity to N_2, which is almost 100% for Pd(0.15)-HMOR, is decreasing with the increase of Pd loading (Fig. 4d).

The best catalytic performance can be achieved by maximising both NO_x total conversion and NO_x selectivity to N_2. However, these two parameters evolve in opposite directions, when Pd loading is increased. At 500 °C, total NO_x conversion has increased with Pd loading, but N_2O formation is being promoted instead of N_2. In fact, above 0.3 wt.% Pd, catalysts present lower NO_x conversion in N_2 than Pd(0.3)-HMOR. On the other hand, though Pd(0.15)-HMOR presents a very high NO_x selectivity to N_2, the conversion is considerably lower when compared, for instance, with Pd(0.3)-HMOR. Based on these data, one can suggest that the 0.3 wt.% Pd loading corresponds to the optimal loading.

Pd^{2+} ions have been identified in previous studies as active species for NO_x CH_4-SCR in different Pd-based catalysts. For instance, Marques et al. [47] concluded that Pd^{2+} surrounded by oxygen atoms is the active site for deNO_x process using methane as reductant and Pd on alumina as the catalysts. The same conclusion was made for bimetallic formulations, *e.g.* Pd/Co-alumina [48]. Characterisation data presented herein for Pd-MOR catalysts indicate that palladium is dispersed as Pd^{2+} in two different ion-exchange positions. The distribution of Pd^{2+} between these two sites appears to be independent of the Pd loading. It is likely that these two types of cations would interact differently with the reactants, and therefore, would have different reactivity. Indeed, Kaucký et al. [49] concluded that cobalt cations located in different positions of the MOR and FER zeolites have different activity for NO_x CH_4-SCR.

Palladium-loaded catalysts are also used as hydrocarbon oxidation catalysts [50,51] and the direct combustion of CH_4 is increasing with Pd loading, which has been also confirmed in this work (Fig. 4c). However, this increase in CH_4 conversion is often associated with the presence of PdO species, which is not the case for the catalysts studied in this work. Instead, one of the Pd^{2+} species may play a role in CH_4 combustion. One of these species may be involved in the formation of N_2O and in the direct combustion of CH_4. Descorme, et al. [52] have presented evidences for the existence of two different nitrosyl complexes formed with Pd cations in different locations of MOR zeolite. Pd mononitrosyl complexes located in the main channels of MOR would be responsible for the NO_x SCR activity, whereas Pd dinitrosyl complexes formed in the side pocket of MOR would be inactive in this reaction. Though no evidence pointed at involvement of Pd located in side pockets in the N_2O formation or CH_4 combustion, one cannot exclude this possibility in the light of the results herein presented.

3.2. The enhancing effect of cerium

3.2.1. Temperature programmed reduction under H_2 (H_2-TPR)

Three groups of reduction peaks have been identified in H_2-TPR profiles of Pd(0.3)Ce(x)-HMOR (Fig. 5): (i) between ~70 and 220, (ii) ~225 and 560 and (iii) ~560 and 920 °C (Table 4). As for Pd(x)-HMOR, the first peak, attributed to the reduction of Pd^{2+} cations in different exchange positions, consists of two components, one centred at ~120 °C and the other close to 150 °C. As the Ce loading increases, the second component becomes more prominent and appears to shift to higher temperatures. For samples with the Ce content over 2 wt.%, the integration of the peaks in the region 70–220 °C yields the H_2/Pd ratio greater than one. This can be explained by the presence of surface Ce^{4+} species, which are reduced in this temperature range [53].

The second reduction peak can be identified between ~225–560 °C in all catalysts containing Ce. This peak is attributed to the reduction of CeO_2 species interacting with Pd [54]. This interaction between species is typical for ceria, which is known to form "bronzes" with noble metals, namely with Pd [53].

An additional broad reduction peak is observed in the TPR profile of Pd(0.3)Ce(10)-HMOR at 560–920 °C. This peak is attributed to the reduction of bulk CeO_2 [53]. For this sample, the existence of higher amounts of CeO_2 species can be explained by the very high loading of Ce. A broad reduction peak corresponding to this species can be

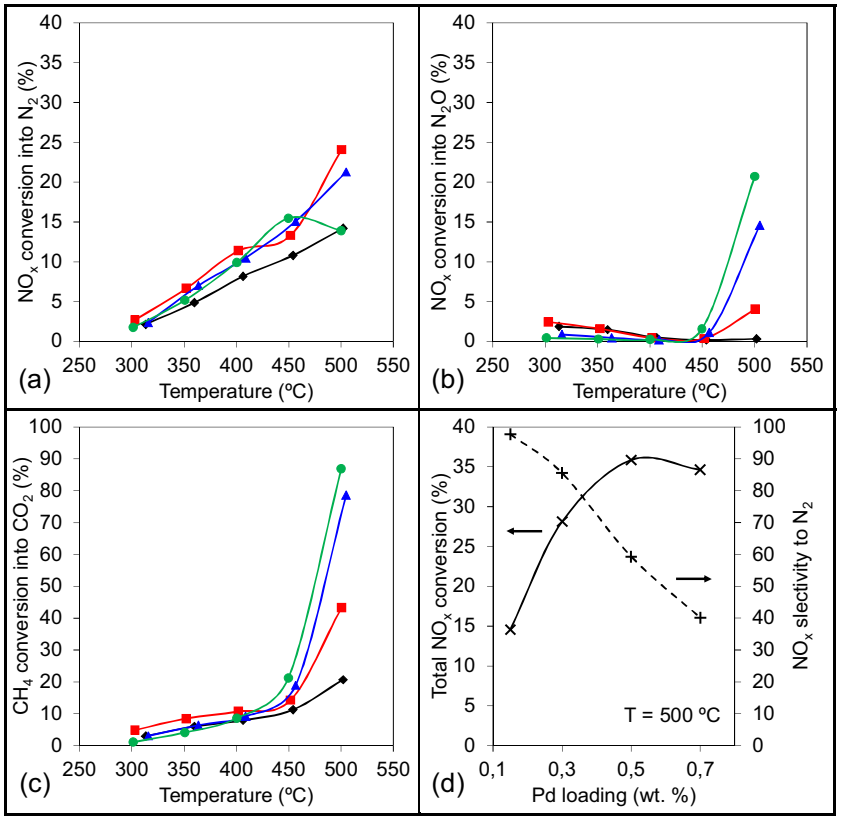

Fig. 4. NO_x CH_4-SCR catalytic test results for Pd(0.15)-HMOR (♦), Pd(0.3)-HMOR (■), Pd(0.5)-HMOR (▲) and Pd(0.7)-HMOR (●): NO_x conversion into N_2 (a) and into N_2O (b), CH_4 conversion into CO_2 (c), and total NO_x conversion and NO_x selectivity to N_2 as function of Pd loading (d). Conditions: 1000 ppm NO, 1000 ppm CH_4, 7 vol.% O_2 and GHSV of 40000 h^{-1}.

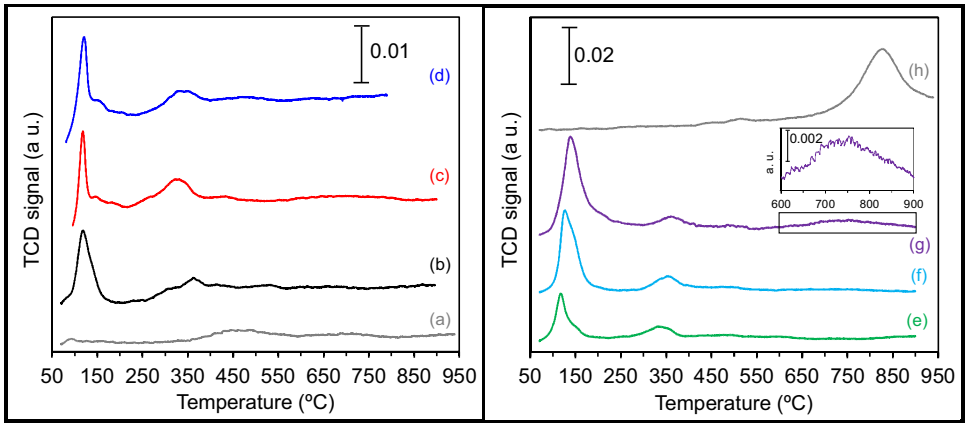

Fig. 5. H_2-TPR profile of PdCe-HMOR catalysts with different Ce loadings: Ce(2)-HMOR (a), Pd(0.3)-HMOR (b), Pd(0.3)Ce(1)-HMOR (c), Pd(0.3)Ce(2)-HMOR (d), Pd(0.3)Ce(3)-HMOR (e), Pd(0.3)Ce(5)-HMOR (f), Pd(0.3)Ce(10)-HMOR (g) and CeO_2/HMOR (h).

Table 4
Peak integration of H_2-TPR profiles of Pd(0.3)Ce(x)-HMOR (x = 1, 2, 3, 5 and 10).

	Peak 1			Peak 2			Peak 3		
	T (°C)	H_2/Pd	μmol H_2 /$g_{catal.}$	T (°C)	H_2/Ce	μmol H_2 /g_{catal}	T (°C)	H_2/Ce	μmol H_2 /g_{catal}
Pd(0.3)Ce(1) –HMOR	100–210	1.0	32	250–560	0.39	22	–	–	–
Pd(0.3)Ce(2) –HMOR	95–215	1.4	39	240–560	0.27	37	–	–	–
Pd(0.3)Ce(3) –HMOR	70–220	1.4	50	225–560	0.14	29	–	–	–
Pd(0.3)Ce(5) –HMOR	75–220	4.1	103	250–560	0.10	35	–	–	–
Pd(0.3)Ce(10) –HMOR	70–270	6.0	152	290–560	0.02	15	560–920	0.06	41

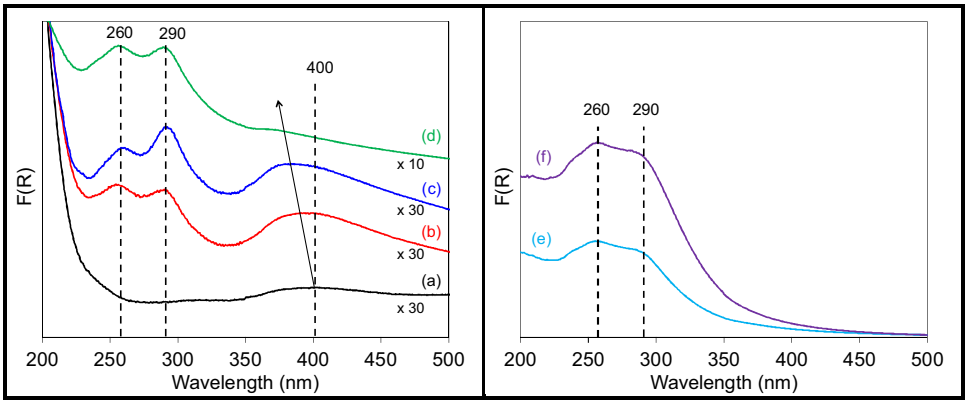

Fig. 6. DRS UV–Vis spectra of PdCe-HMOR catalysts containing 0.3 wt.% of Pd and different loadings of Ce: Pd(0.3)-HMOR (a), Pd(0.3)Ce(1)-HMOR (**b**) Pd(0.3)Ce(2)-HMOR (**c**), Pd(0.3)Ce(3)-HMOR (**d**), Pd(0.3)Ce(5)-HMOR (**e**) and Pd(0.3)Ce(10)-HMOR (**f**).

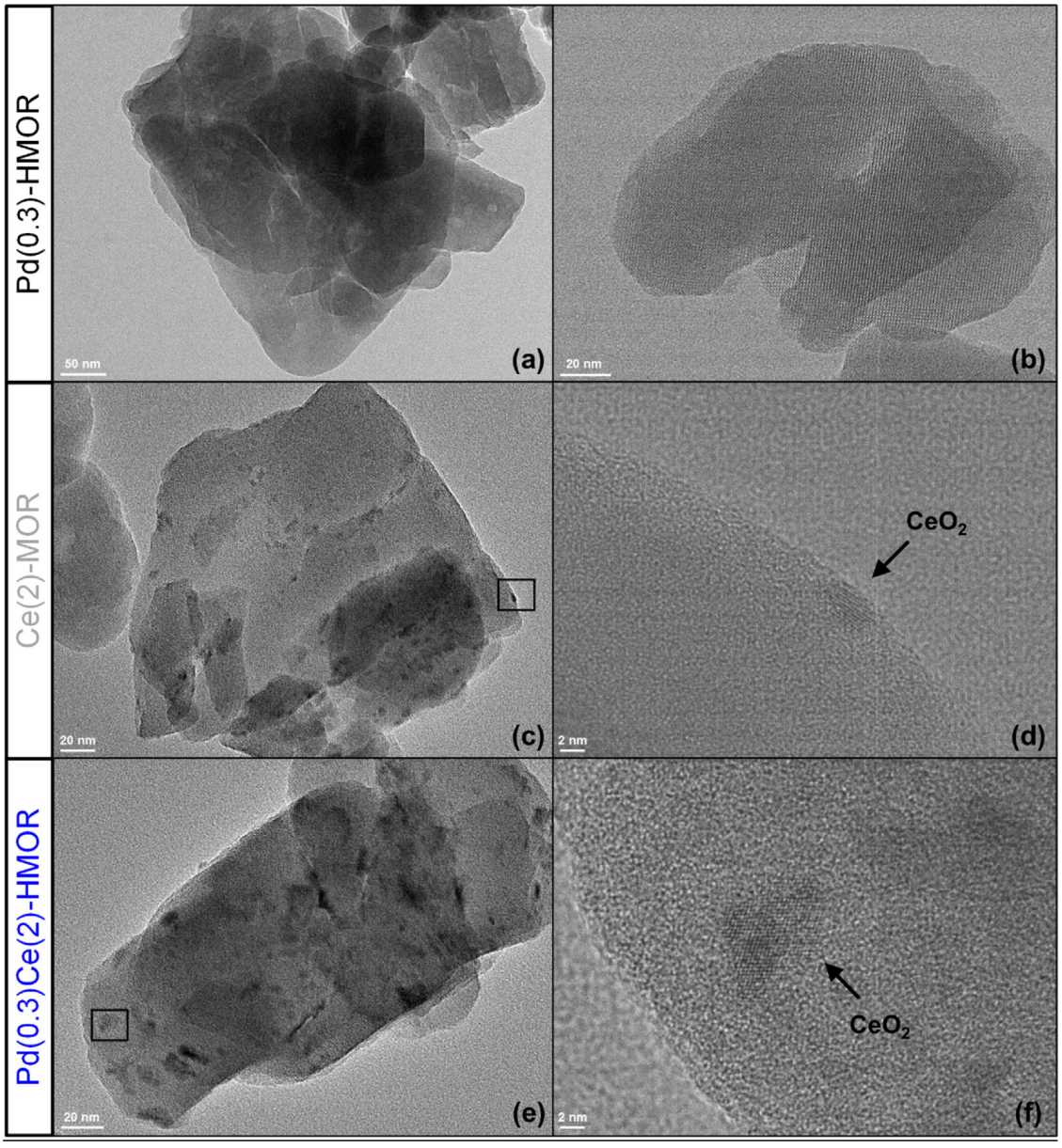

Fig. 7. TEM images: Pd(0.3)-HMOR (a,b), Ce(2)-HMOR(c,d) and Pd(0.3)Ce(2)-HMOR (e,f).

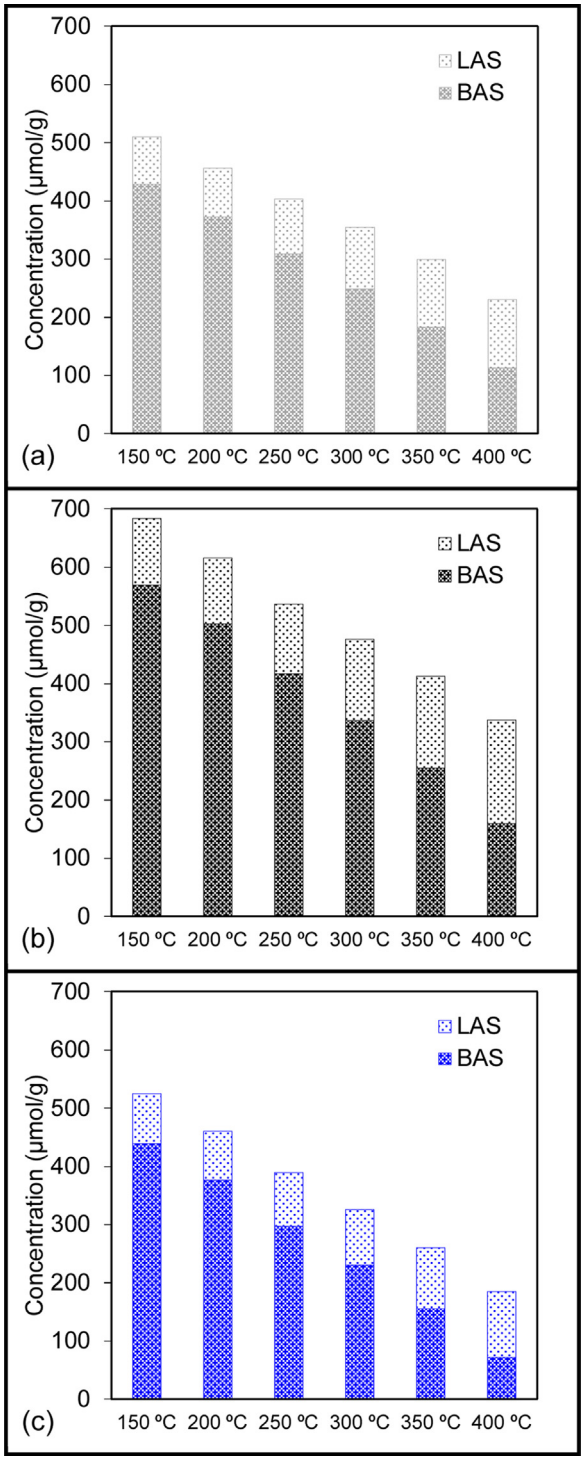

Fig. 8. Quantification of acid sites of HMOR (a), Pd(0.3)-HMOR (b) and Pd(0.3)Ce(2)-HMOR (c) using pyridine thermodesorption followed by FTIR.

clearly observed in the reduction profile of CeO_2/HMOR sample, obtained by mechanical mixture of bulk CeO_2 with HMOR zeolite in proportion 1:2.

3.2.2. Diffuse reflectance UV–Vis spectroscopy (DRS UV–Vis)

DRS UV–Vis spectra of the Pd(0.3)-HMOR and Pd(0.3)Ce(x)-HMOR (x = 1, 2, 3, 5 and 10) are presented in Fig. 6. For the bimetallic catalysts, two bands between 250 and 300 nm can be attributed to cerium species: the first band, at 260 nm, corresponds to the 4f-5d transition in Ce^{3+} [55,56], and the second band, at 290 nm, is characteristic of the charge transfer from O^{2-} to Ce^{4+} in CeO_2 clusters [56]. The intensity of both bands increases with Ce loading. Furthermore, the increase in the Ce loading causes a blue-shift in the band around 400 nm attributed to the Pd^{2+} species, which might result from the interaction between Pd and Ce species that has also been observed in H_2-TPR. For Ce loadings above 5 wt.%, the bands corresponding to Ce species become so intense that it is no longer possible to clearly observe the band around 400 nm.

3.2.3. Transmission electron microscopy (TEM/EDS)

TEM images for Pd(0.3)-HMOR, Ce(2)-HMOR and Pd(0.3)Ce(2)-HMOR are presented in Fig. 7. For Pd(0.3)-HMOR, no metal particles are observed in the TEM images collected (Fig. 7a,b). Additionally, energy-dispersive X-ray spectroscopy (EDS) analyses do not detect palladium in the sample. The detection limit of this technique does not allow to detect low amounts of Pd in samples where it is well dispersed.

For Ce(2)-HMOR, several Ce-containing clusters can be observed in TEM images (Fig. 7c). These clusters have irregular shapes, their estimated size (~10 nm) is about one order of magnitude smaller than the zeolite particle size (~100 nm). High resolution TEM and EDS analyses confirm these are CeO_2 clusters with the lattice d-spacing of 2.7 and 3.1 Å (ICDD 00-034-0394). Similar CeO_2 clusters have been observed in Pd(0.3)Ce(2)-HMOR and Ce(2)-HMOR, but no Pd particles have been identified indicating a high degree of palladium dispersion in the zeolite framework after cerium introduction.

3.2.4. Quantification of acid sites by pyridine-FTIR spectroscopy

The role of zeolite Brønsted acid sites (BAS) in NO_x CH_4-SCR has been widely studied and reported in literature [40,57–59]. The results of acidity measurements carried out in this work are presented in Fig. 8. The data show that Pd(0.3)-HMOR has a significantly higher number of BAS (503 µmol/g, 200 °C) as compared to both HMOR (372 µmol/g, 200 °C) and Pd(0.3)Ce(2)-HMOR (377 µmol/g, 200 °C). This could be related to partial dihydroxylation or restricted access of pyridine to acid sites resulted from the calcination of the latter two samples at 500 °C for an extended period of time. As the maximum rate of Pd^{2+} exchange in Pd(0.3)Ce(2)-HMOR is below 4% (Table 2), it should not significantly affect the number of BAS. In contrast, if a considerable part of cerium was stabilised as Ce^{3+} during ion exchange, one would expect a significant decrease on acidity, since the maximum exchange rate of Ce in Pd(0.3)Ce(2)-HMOR is around 30%. The fact that HMOR and Pd(0.3)Ce(2)-HMOR present similar values of BAS indirectly confirms that Ce^{3+} ions are not the predominant Ce species stabilised in the zeolite matrix. Indeed, according to the TEM data, CeO_2 is formed during the catalysts preparation and high temperature treatment.

3.2.5. CO adsorption followed by FTIR spectroscopy

FTIR spectra of CO adsorbed on HMOR, Pd(0.3)-HMOR, Pd(0.3)Ce(2)-HMOR and Ce(2)-HMOR are compared in Fig. 9. In the spectra of Pd(0.3)Ce(2)-HMOR and Ce(2)-HMOR an intense band is observed at 2188 cm^{-1} that can be attributed to Ce^{n+}-CO complexes (Ce^{3+} or Ce^{4+}) [44], which have been previously identified by DRS UV–Vis spectroscopy. An additional band is also observed at 2123 cm^{-1}, which has not been found in Pd(0.3)-HMOR and Ce(2)-HMOR. This band can be assigned to either Ce^{n+}-CO or Pd^{n+}-CO species (2215–2110 cm^{-1} spectral range) not present in the monometallic catalysts.

The band at 2290 cm^{-1} is ascribed to CO_2 complexes formed due to CO oxidation, it appears together with an intense band at 2355 cm^{-1} attributed to linear CO_2 [60] (not shown). These bands

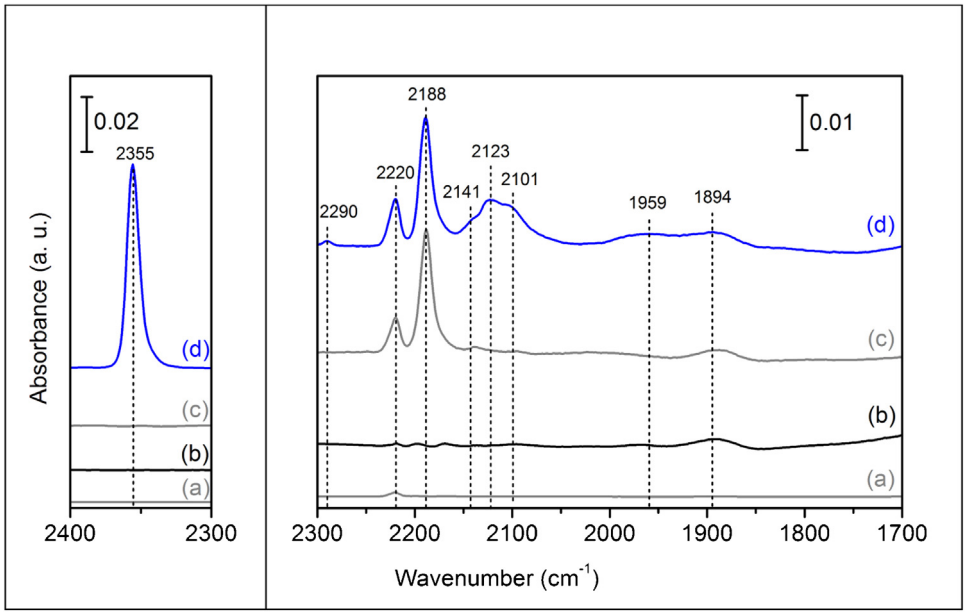

Fig. 9. FTIR spectra of reduced catalysts at room temperature, after CO exposure to 5 torr: HMOR (a), Pd(0.3)-HMOR (**b**), Ce(fx7)-HMOR (**c**) and Pd(0.3)Ce(2)-HMOR (**d**).

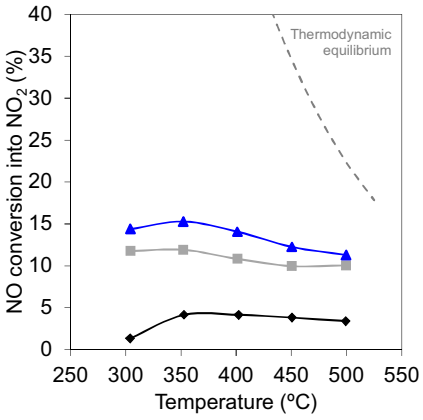

Fig. 10. Conversion of NO into NO_2 for Pd(0.3)-HMOR (♦), Ce(2)-HMOR (■) and Pd(0.3)Ce(2)-HMOR (▲). Conditions: 1000 ppm NO, 7 vol.% O_2 and GHSV of 40000 h^{-1}.

only appear in the bimetallic catalyst, which suggests that CO oxidation seems to require the presence of both Pd and Ce species. The band at ~1888 cm^{-1} is probably related to the formation of carbonate species.

The bands at 2141, 2101, 1959 and 1894 cm^{-1} in Pd(0.3)-HMOR can be attributed to CO adsorbed on the Pd species previously described for monometalic PdMOR samples.

3.2.6. NO oxidation

Oxidation of NO to NO_2 is considered to be the first key step in the NO_x SCR reaction involving hydrocarbons as reducing agents [61–63]. Fig. 10 shows conversion of NO into NO_2 as a function of temperature in the absence of methane (the hydrocarbon reducing agent). The oxidation activity increases in the order Pd(0.3)-HMOR < Ce(2)-HMOR < Pd(0.3)Ce(2)-HMOR. This suggests that Ce species play a role in promoting NO conversion over Pd(0.3)Ce(2)-HMOR and could also act to enhance the catalytic performance of this catalyst in NO_x CH_4-SCR by oxidising NO to NO_2 [34].

The role of Ce as oxidation promoter has also been confirmed by FTIR-CO, as the formation of CO_2 complexes on Pd(0.3)Ce(2)-HMOR, resulting from the CO oxidation, has been detected in the infrared spectra. However, this phenomenon has not been observed for the monometallic formulations.

3.2.7. Active species in Pd/Ce-HMOR for NO_x CH_4-SCR

The enhancing effect of Ce on NO_x CH_4-SCR has been assessed by testing the Pd(0.3)Ce(x)-HMOR catalysts in comparison to Pd(0.3)-HMOR and Ce(2)-HMOR (Fig. 11; N_2O and CO formation is negligible and is not presented).

Ce(2)-HMOR is practically inactive in the NO_x CH_4-SCR reaction up to 450 °C. Even at 500 °C, NO_x conversion value is only 6%, which is significantly lower than for Pd(0.3)-HMOR (24%). At lower temperatures, 300–350 °C, all Pd-based catalysts present similar NO_x and CH_4 conversion. However above 350 °C, the addition 1–5 wt.% Ce leads to an increase in NO_x conversion. For Ce loadings of 1 and 2 wt.%, NO_x conversion increases with the reaction temperature, whereas for 3 and 5 wt.% loadings, maximum NO_x conversion is reached at 450 °C. This behaviour can be explained by the lack of CH_4, since its conversion is over 80% at 500 °C.

An important indicator of the catalyst performance is its efficiency in using CH_4 to reduce NO_x. When 1 wt.% Ce is added to Pd(0.3)-HMOR, the selectivity of methane to SCR reaction increases. For higher Ce loadings, the selectivity becomes lower than that for Pd(0.3)-HMOR; however, there is also a significant difference in the NO_x conversion to N_2.

The catalytic behaviour of the catalyst with the highest Ce content, Pd(0.3)Ce(10)-HMOR, changes considerably: both the NO_x and CH_4 conversions decrease, probably because Ce-containing species are poorly dispersed in the zeolite structure. Indeed, the NO_x conversion is similar for Pd(0.3)Ce(10)-HMOR and Pd(0.3)-HMOR that was mechanically mixed with bulk CeO_2 in order to obtain a similar Ce loading in the sample, *ca.* 10 wt.%-Pd(0.3)Ce(10)-HMOR(MM), for which one would expect a low cerium dispersion with larger CeO_2 particles present on the external surface of the

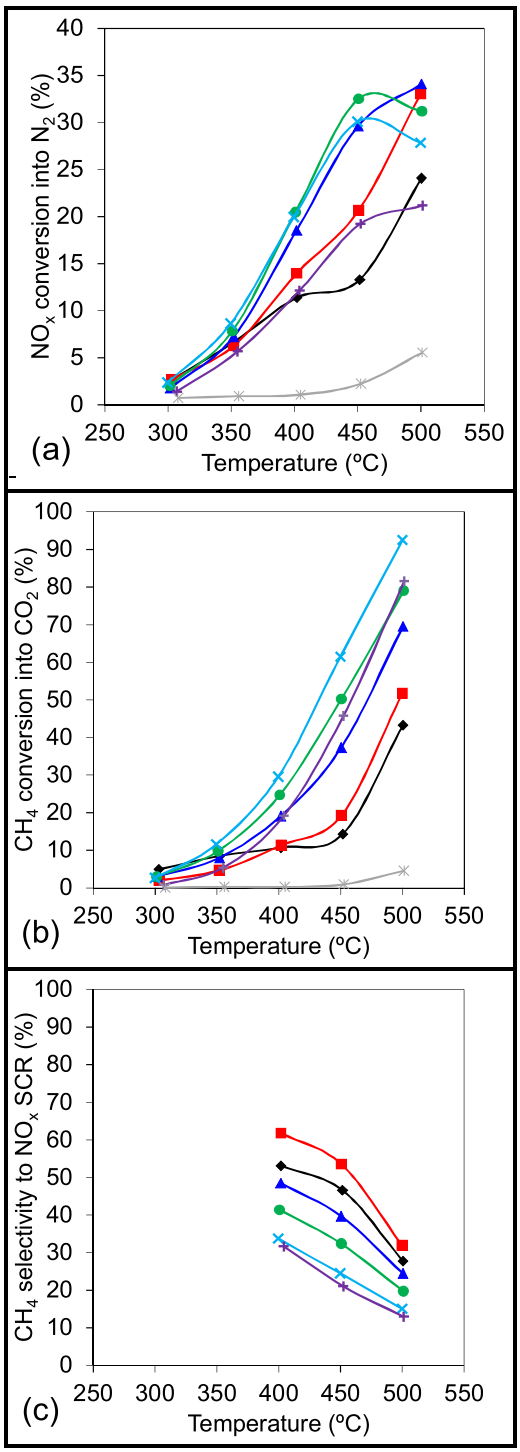

Fig. 11. NO_x CH_4-SCR catalytic test results for Pd(0.3)-HMOR (♦), Pd(0.3)Ce(1)-HMOR (■), Pd(0.3)Ce(2)-HMOR (▲), Pd(0.3)Ce(3)-HMOR (●), Pd(0.3)Ce(5)-HMOR (X), Pd(0.3)Ce(10)-HMOR (✚) and Ce(2)-HMOR(✱): NO_x conversion into N_2 (a), CH_4 conversion into CO_2 (b) and CH_4 selectivity to NO_x SCR reaction (c). Conditions: 1000 ppm NO, 1000 ppm CH_4, 7% O_2 and GHSV of 40000 h^{-1}.

zeolite (Fig. 12). H_2-TPR profile of Pd(0.3)Ce(10)-HMOR(MM) is presented in the supplementary data showing the reduction of bulk CeO_2 at high temperature.

Although Ce(2)-HMOR is practically inactive in NO_x CH_4-SCR reaction and in the direct combustion of methane, this catalyst shows moderate conversion values for NO oxidation to NO_2, which are higher than those for Pd(0.3)-HMOR. Therefore, it can be suggested that the role of cerium species is to promote the oxidation of NO, which is in agreement with the data previously reported in the literature [34,64]. Several mechanisms proposed for the HC-SCR reaction indicate that NO oxidation to NO_2 is the first key step in the HC-SCR reaction. This work provides important details regarding Ce species promoting NO oxidation over zeolite-based catalysts. TEM/EDS and H_2-TPR indicate that these are well dispersed CeO_2 oxide clusters observed in the catalysts with a moderate Ce loading, *e.g.* Pd(0.3)Ce(2)-HMOR. H_2-TPR, DRS UV–Vis and FTIR-CO also show that Pd and Ce species interact with each other, which might be the key for the promotion of $deNO_x$ process.

For Pd(0.3)Ce(x)-HMOR catalysts, the quantification of the second reduction peak in H_2-TPR profiles results in a higher H_2/Ce ratio for Pd(0.3)Ce(1)-HMOR, and the CH_4 selectivity towards SCR follows the same trend. The H_2/Ce ratio corresponding to this reduction process can be seen as an indicator of the relative amount of cerium species interacting with palladium species, and the total amount of H_2 consumed in the reduction process is directly related to the absolute amount of Ce species interacting with Pd species. A decrease in the H_2/Ce ratio with increasing Ce loading represents an increase in the number of Ce species not interacting with Pd, which would favour the direct combustion of methane.

The results suggest that the balance between the number of CeO_2 species interacting with Pd and those not interacting with it plays a crucial role in the catalytic performance of PdCe-HMOR in NO_x CH_4-SCR. For the catalyst containing 0.3 wt.% Pd and 2 wt.% Ce, the optimal Pd/Ce species distribution is obtained, resulting in the best catalytic performance in the SCR reaction studied in this work.

4. Conclusions

The role of palladium and cerium species in the NO_x CH_4-SCR reaction has been evaluated using mordenite catalysts containing Pd and Ce. These monometallic and bimetallic systems have been characterised by H_2-TPR, DRS UV–vis, TEM/EDS, FTIR and their catalytic performance in NO oxidation and CH_4-SCR has been investigated.

The increase in palladium loading in Pd-HMOR leads to a decrease in NO_x selectivity towards N_2, favouring N_2O formation. The addition of cerium to Pd-HMOR enhances the catalytic performance for NO_x CH_4-SCR. By adding 1 wt.% Ce, both NO_x conversion into N_2 and CH_4 selectivity towards SCR reaction are increased. However, for Ce loading above 3 wt.%, the direct combustion of methane is strongly favoured, in particular at high temperatures, resulting in a declining NO_x CH_4-SCR performance.

Pd^{2+} ions in exchange position are active species for $deNO_x$ process. CeO_2 species play an important role in the NO oxidation to NO_2, which is considered as the first key step in the HC-SCR reaction. For PdCe-HMOR system, the existence of small CeO_2 clusters interacting with Pd species leads to the enhanced catalytic performance. It appears that the balance between CeO_2 species interacting with Pd and those which do not is an important parameter influencing the capacity of PdCe-HMOR catalysts to effectively use CH_4 as the reducing agent in the $deNO_x$ process.

Acknowledgements

The authors acknowledge Fundação para a Ciência e a Tecnologia (FCT)–project UID/QUI/00100/2013 and grant SFRH/BD/78639/2011-and ENGIE for financial support(project ENGIE/IST/UPMC).

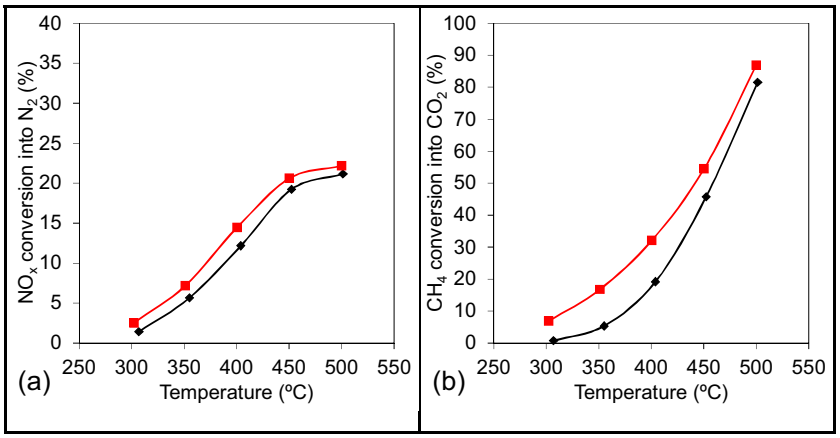

Fig. 12. NO_x CH_4-SCR catalytic test results for Pd(0.3)Ce(10)-HMOR(IWI) (♦) and Pd(0.3)Ce(10)-HMOR(MM) (■): NO_x conversion into N_2 (a) and CH_4 conversion into CO_2 (b). Conditions: 1000 ppm NO, 1000 ppm CH_4, 7% O_2 and GHSV of 40000 h^{-1}.

Appendix A. Supplementary data

Supplementary data associated with this article can be found, in the online version, at http://dx.doi.org/10.1016/j.apcatb.2016.05.004.

References

[1] European Union, Website, Emissions of Nitrogen Oxides (NOx) by Source Sector, http://ec.europa.eu/eurostat/web/products-datasets/-/tsdpc270, (accessed in June 2015).
[2] DieselNet, website, http://www.dieselnet.com/standards/#eu, (accessed in 08.03.13).
[3] P. Granger, V.I. Parvulescu, Chem. Rev. 111 (2011) 3155–3207.
[4] B.C. Choi, D.E. Foster, J. Ind. Eng. Chem. 11 (2005) 1–9.
[5] NGV Global, website, Current Natural Gas Vehicle Statistics, http://www.iangv.org/current-ngv-stats/, (accessed in June 15).
[6] Y.J. Li, J.N. Armor, Appl. Catal. B 1 (1992) L31–L40.
[7] Y.J. Li, J.N. Armor, J. Catal. 150 (1994) 376–387.
[8] Y.J. Li, T.L. Slager, J.N. Armor, J. Catal. 150 (1994) 388–399.
[9] J. Dedecek, D. Kaucky, B. Wichterlova, Top. Catal. 18 (2002) 283–290.
[10] L.B. Gutierrez, E.E. Miro, M.A. Ulla, Appl. Catal. A 321 (2007) 7–16.
[11] F. Lonyi, H.E. Solt, Z. Paszti, J. Valyon, Appl. Catal. B 150 (2014) 218–229.
[12] M. Ogura, Y. Sugiura, M. Hayashi, E. Kikuchi, Catal. Lett. 42 (1996) 185–189.
[13] F. Bustamante, F. Cordoba, M. Yates, C.M. de Correa, Appl. Catal. A 234 (2002) 127–136.
[14] J.A.Z. Pieterse, R.W. van den Brink, S. Booneveld, F.A. de Bruijn, Appl. Catal. B 39 (2002) 167–179.
[15] A.P. Ferreira, C. Henriques, M.F. Ribeiro, F.R. Ribeiro, Catal. Today 107–108 (2005) 181–191.
[16] A.P. Ferreira, S. Capela, P. Da Costa, C. Henriques, M.F. Ribeiro, F.R. Ribeiro, Catal. Today 119 (2007) 156–165.
[17] S. Capela, R. Catalao, P. Da Costa, G. Djega-Mariadassou, F.R. Ribeiro, F. Ribeiro, C. Henriques, Zeolites and Related Materials: Trends, Targets and Challenges, in: A.M.P.B.F. Gedeon (Ed.), Proceedings of the 4th International Feza Conference (2008) 1033–1038.
[18] A. Rodrigues, P. da Costa, C. Methivier, S. Dzwigaj, Catal. Today 176 (2011) 72–76.
[19] L. Gutierrez, A. Boix, J.O. Petunchi, J. Catal. 179 (1998) 179–191.
[20] F. Lonyi, J. Valyon, L. Gutierrez, M.A. Ulla, E.A. Lombardo, Appl. Catal. B 73 (2007) 1–10.
[21] A. Kubacka, J. Janas, B. Sulikowski, Appl. Catal. B 69 (2006) 43–48.
[22] F. Lonyi, H.E. Solt, J. Valyon, A. Boix, L.B. Gutierrez, J. Mol. Catal. A: Chem. 345 (2011) 75–80.
[23] F. Lonyi, H.E. Solt, J. Valyon, A. Boix, L.B. Gutierrez, Appl. Catal. B 117 (2012) 212–223.
[24] L. Gutierrez, E.A. Lombardo, Appl. Catal. A 360 (2009) 107–119.
[25] L.L. Ren, T. Zhang, D.B. Liang, C.H. Xu, J.W. Tang, L.W. Lin, Appl. Catal. B 35 (2002) 317–321.
[26] A. Chen, C.T. Zhu, Catal. Lett. 141 (2011) 207–212.
[27] P. Ciambelli, D. Sannino, E. Palo, A. Ruggiero, Top. Catal. 42-43 (2007) 177–181.
[28] European Chemicals Agency, Website, Candidate List of Substances of Very High Concern for Authorisation http://echa.europa.eu/candidate-list-table, (accessed in June 2015).
[29] Y. Nishizaka, M. Misono, Chem. Lett. (1993) 1295–1298.
[30] C.M. de Correa, F. Córdoba, C.F. Bustamante, L. in: F.V.M.S.M. Avelino Corma, G.F. José Luis (Eds.) Studies in Surface Science and Catalysis, Elsevier, 2000, pp. 1469–1474.
[31] H. Decolatti, H. Solt, F. Lonyi, J. Valyon, E. Miro, L. Gutierrez, Catal. Today 172 (2011) 124–131.
[32] F. Lonyi, H.E. Solt, J. Valyon, H. Decolatti, L.B. Gutierrez, E. Miro, Appl. Catal. B 100 (2010) 133–142.
[33] J.A.Z. Pieterse, R.W. van den Brink, S. Booneveld, F.A. de Bruijn, in: E. VanSteen, M. Claeys, L.H. Callanan (Eds.), Recent Advances in the Science and Technology of Zeolites and Related Materials, 2004, pp. 2522–2526.
[34] J.A.Z. Pieterse, S. Booneveld, Appl. Catal. B 73 (2007) 327–335.
[35] I.O. Costilla, M.D. Sanchez, M. Alicia Volpe, C.E. Gigola, Catal. Today 172 (2011) 84–89.
[36] C.A. Emeis, J. Catal. 141 (1993) 347–354.
[37] F. Thibault-Starzyk, B. Gil, S. Aiello, T. Chevreau, J.P. Gilson, Microporous Mesoporous Mater. 67 (2004) 107–112.
[38] S.N. Reifsnyder, M.M. Otten, H.H. Lamb, Catal. Today 39 (1998) 317–328.
[39] A.M. De Oliveira, I. Costilla, C. Gigola, I.M. Baibich, V.T. da Silva, S.B.C. Pergher, Catal. Lett. 136 (2010) 185–191.
[40] B.J. Adelman, W.M.H. Sachtler, Appl. Catal. B 14 (1997) 1–11.
[41] J. Dedecek, B. Wichterlova, J. Phys. Chem. B 103 (1999) 1462–1476.
[42] W.J. Mortier, Compilation of Extra Framework Sites in Zeolites, Butterworth Scientific Limited, 1982.
[43] R. Grybos, J. Hafner, L. Benco, H. Toulhoat, J. Phys. Chem. C 111 (2007) 6454–6464.
[44] K.I. Hadjiivanov, G.N. Vayssilov, Adv. Catal. 47 (2002) 307–511.
[45] V. Gruver, J.J. Fripiat, J. Phys. Chem. 98 (1994) 8549–8554.
[46] M. Armandi, B. Bonelli, E. Garrone, M. Ardizzi, F. Cavani, L. Dal Pozzo, L. Maselli, R. Mezzogori, G. Calestani, Appl. Catal. B 70 (2007) 585–596.
[47] R. Marques, L. Mazri, S. Da Costa, F. Delacroix, G. Djega-Mariadassou, P. Da Costa, Catal. Today 137 (2008) 179–184.
[48] R. Marques, L. Mazri, S. Da Costa, F. Delacroix, G. Djega-Mariadassou, P. Da Costa, Catal. Today 137 (2008) 185–190.
[49] D. Kaucky, A. Vondrova, J. Dedecek, B. Wichterlova, J. Catal. 194 (2000) 318–329.
[50] P. Gelin, M. Primet, Appl. Catal. B 39 (2002) 1–37.
[51] Y.J. Li, J.N. Armor, Appl. Catal. B 3 (1994) 275–282.
[52] C. Descorme, P. Gélin, C. Lécuyer, M. Primet, J. Catal. 177 (1998) 352–362.
[53] A. Trovarelli, Cat. Rev.-Sci. Eng. 38 (1996) 439–520.
[54] Y.-S. Bi, G.-Y. Dang, X.-H. Zhao, X.-F. Meng, H.-J. Lu, J.-T. Jin, J. Hazard. Mater. 229–230 (2012) 245–250.
[55] L.F. Cordoba, M. Flytzani-Stephanopoulos, C.M. de Correa, Appl. Catal. B 33 (2001) 25–33.
[56] Z.J. Li, M. Flytzani-Stephanopoulos, J. Catal. 182 (1999) 313–327.
[57] J.T. Miller, E. Glusker, R. Peddi, T. Zheng, J.R. Regalbuto, Catal. Lett. 51 (1998) 15–22.
[58] C.J. Loughran, D.E. Resasco, Appl. Catal. B 7 (1995) 113–126.
[59] Y. Nishizaka, M. Misono, Chem. Lett. (1994) 2237–2240.
[60] M. Daturi, C. Binet, J.C. Lavalley, A. Galtayries, R. Sporken, Phys. Chem. Chem. Phys. 1 (1999) 5717–5724.
[61] G. Djega-Mariadassou, Catal. Today 90 (2004) 27–34.
[62] O. Gorce, F. Baudin, C. Thomas, P. Da Costa, G. Djega-Mariadassou, Appl. Catal. B 54 (2004) 69–84.
[63] A. Lamacz, A. Krzton, G. Djega-Mariadassou, Appl. Catal. B 142 (2013) 268–277.
[64] T. Liese, E. Loffler, W. Grunert, J. Catal. 197 (2001) 123–130.